Flexible inkjet-printed metamaterial absorber for coating a cylindrical object

Hyung Ki Kim, Kenyu Ling, Kyeongseob Kim, and Sungjoon Lim*

Laboratory of Electromagnetics and Optics, School of Electrical and Electronic Engineering, Chung-Ang University, Heukseok-Dong, Dongjak-Gu 156-756 Seoul, South Korea
sungjoon@cau.ac.kr

Abstract: In this paper, a novel flexible inkjet-printed metamaterial absorber is proposed. The unit cell of the metamaterial is designed with a modified Jerusalem-cross ring resonator and is inkjet printed with silver nanoparticle ink on a flexible polymer film. All fabrication processes are performed using a commercial printer (EPSON WF-7011). The absorber's flexibility and absorption performance are demonstrated by measuring the absorption ratio after coating the proposed absorber on a cylindrical object with a radius of 4.56 cm. An absorption rate exceeding 99% is achieved at 9.21 GHz for both flat and cylindrical surfaces. In addition, the cylindrical model attains an absorption rate higher than 96% for all polarization angles, and a high absorption rate of 95% is preserved until the incident angle is less than 30þ.

OCIS codes: (160.3918) Metamaterials; (260.5740) Resonance; (050.6624) Subwavelength structures.

References and links

1. Z. Liu, G. Bai, Y. Huang, Y. Ma, F. Du, F. Li, T. Guo, and Y. Chen, "Reflection and absorption contributions to the electromagnetic interference shielding of single-walled carbon nanotube/polyurethane composites," Carbon **45**(4), 821–827 (2007).
2. Y. Takimoto, Considerations on millimeter-wave indoor LAN" in Millimeter Waves, 1997 Topical Symposium on Anonymous (IEEE, 1997).
3. K. Iwaszczuk, A. C. Strikwerda, K. Fan, X. Zhang, R. D. Averitt, and P. U. Jepsen, "Flexible metamaterial absorbers for stealth applications at terahertz frequencies," Opt. Express **20**(1), 635–643 (2012).
4. N. I. Landy, S. Sajuyigbe, J. J. Mock, D. R. Smith, and W. J. Padilla, "Perfect metamaterial absorber," Phys. Rev. Lett. **100**(20), 207402 (2008).
5. P. K. Singh, K. A. Korolev, M. N. Afsar, and S. Sonkusale, "Single and dual band 77/95/110 GHz metamaterial absorbers on flexible polyimide substrate," Appl. Phys. Lett. **99**(26), 264101 (2011).
6. H. Tao, A. C. Strikwerda, K. Fan, W. J. Padilla, X. Zhang, and R. D. Averitt, "MEMS based structurally tunable metamaterials at terahertz frequencies," J. Infrared Millim. THz Waves **32**(5), 580–595 (2011).
7. N. Landy, C. Bingham, T. Tyler, N. Jokerst, D. Smith, and W. Padilla, "Design, theory, and measurement of a polarization-insensitive absorber for terahertz imaging," Phys. Rev. B **79**(12), 125104 (2009).
8. H. Tao, C. Bingham, D. Pilon, K. Fan, A. Strikwerda, D. Shrekenhamer, W. Padilla, X. Zhang, and R. Averitt, "A dual band terahertz metamaterial absorber," J. Phys. D **43**(22), 225102 (2010).
9. X. Liu, T. Starr, A. F. Starr, and W. J. Padilla, "Infrared spatial and frequency selective metamaterial with near-unity absorbance," Phys. Rev. Lett. **104**(20), 207403 (2010).
10. N. Liu, M. Mesch, T. Weiss, M. Hentschel, and H. Giessen, "Infrared perfect absorber and its application as plasmonic sensor," Nano Lett. **10**(7), 2342–2348 (2010).
11. J. Hao, J. Wang, X. Liu, W. J. Padilla, L. Zhou, and M. Qiu, "High performance optical absorber based on a plasmonic metamaterial," Appl. Phys. Lett. **96**(25), 251104 (2010).
12. B. Zhu, Z. Wang, C. Huang, Y. Feng, J. Zhao, and T. Jiang, "Polarization insensitive metamaterial absorber with wide incident angle," Prog. Electromagnetics Res. **101**, 231–239 (2010).
13. Q. Wen, H. Zhang, Q. Yang, Z. Chen, Y. Long, Y. Jing, Y. Lin, and P. Zhang, "A tunable hybrid metamaterial absorber based on vanadium oxide films," J. Phys. D **45**(23), 235106 (2012).
14. B. S. Cook and A. Shamim, "Inkjet printing of novel wideband and high gain antennas on low-cost paper substrate," IEEE Trans. Antennas Propagat. **60**(9), 4148–4156 (2012).

#228743 - $15.00 USD Received 28 Nov 2014; revised 30 Jan 2015; accepted 18 Feb 2015; published 25 Feb 2015

15. K. Latti, M. Kettunen, J. Strom, and P. Silventoinen, "A review of microstrip T-resonator method in determining the dielectric properties of printed circuit board materials," IEEE Trans. Instrum. Meas. **56**(5), 1845–1850 (2007).
16. Y. Cheng, H. Yang, Z. Cheng, and N. Wu, "Perfect metamaterial absorber based on a split-ring-cross resonator," Appl. Phys., A Mater. Sci. Process. **102**(1), 99–103 (2011).
17. E. Pshenay-Severin, M. Falkner, C. Helgert, and T. Pertsch, "Ultra broadband phase measurements on nanostructured metasurfaces," Appl. Phys. Lett. **104**(22), 221906 (2014).
18. B. Kanté, J. Lourtioz, and A. de Lustrac, "Infrared metafilms on a dielectric substrate," Phys. Rev. B **80**(20), 205120 (2009).
19. H. Chen, J. Zhang, Y. Bai, Y. Luo, L. Ran, Q. Jiang, and J. A. Kong, "Experimental retrieval of the effective parameters of metamaterials based on a waveguide method," Opt. Express **14**(26), 12944–12949 (2006).
20. D. R. Smith, D. C. Vier, T. Koschny, and C. M. Soukoulis, "Electromagnetic parameter retrieval from inhomogeneous metamaterials," Phys. Rev. E Stat. Nonlin. Soft Matter Phys. **71**(3 3 Pt 2B), 036617 (2005).
21. Z. Bo, W. Zheng-Bin, Y. Zhen-Zhong, Z. Qi, Z. Jun-Ming, F. Yi-Jun, and J. Tian, "Planar metamaterial microwave absorber for all wave polarizations," Chin. Phys. Lett. **26**(11), 114102 (2009).
22. B. Zhu, Z. Wang, C. Huang, Y. Feng, J. Zhao, and T. Jiang, "Polarization insensitive metamaterial absorber with wide incident angle," Prog. Electromagnetics Res. **101**, 231–239 (2010).

1. Introduction

Electromagnetic (EM) absorbers can minimize transmitted and reflected EM waves. These absorbers can be used for various applications, including electromagnetic interference (EMI) [1], wireless communication [2], and stealth technology [3]. Recently, N. Landy et al. introduced metamaterials to design a thin and low-cost EM absorber [4]. Metamaterial-based absorbers show almost perfect absorptivity, despite their thin thickness. Because the effective permittivity and permeability of a metamaterial can be artificially manipulated by an EM resonator (such as a split-ring resonator), we can design the absorber's intrinsic impedance to match the impedance of free space at a specific resonant frequency. In addition, the transmitted EM wave can be absorbed by dissipating EM energy with ohmic and dielectric losses. Recently, metamaterial absorbers have been researched for different portions of the spectrum, such as microwave [1, 2, 4], millimeter wave [5], terahertz [6–8], infrared [9, 10], and optical signals [11]. Because the metamaterial may receive EM waves from either arbitrary incident angles or polarization, it is also necessary to study polarization- and angle-insensitive metamaterial absorbers [12].

Most metamaterial absorbers have been realized on hard substrates, such as FR4 materials [4, 12], silicon [6, 7], and vanadium oxide [13]. As these materials are inflexible, metamaterial absorbers that use hard substrates are limited to planar surfaces. Therefore, a few flexible metamaterial absorbers on a polyimide substrate have been proposed [3, 5, 8]. To fabricate a metamaterial absorber structure on a polyimide substrate, researchers have used traditional mask contact photo-lithography.

In the present study, we design a flexible metamaterial absorber on a polymer film, and the conductive patterns are inkjet-printed using silver nanoparticle inks. Compared with previous lithography fabrication processes, the inkjet printing process is very fast, simple, and inexpensive because we can print the pattern from a graphic file using a home printer. In addition, no chemical waste is generated; consequently, no post-processing is necessary, and no additional costs are incurred. Therefore, inkjet printing technology is very useful for realizing printing on flexible materials, such as polymer film and paper. To demonstrate its flexibility, the inkjet-printed metamaterial absorber is deployed on a cylindrical object in this study.

2. Inkjet-printing process and absorber design

The geometry of the proposed absorber unit cell is shown in Fig. 1. On the top layer of the unit cell, a Jerusalem cross with an additional circular ring pattern is printed using silver nanoparticle ink, and the bottom layer of the unit cell is fully covered with a copper sheet. When the silver nanoparticle ink is printed on the substrate, it forms a silver particle agglomeration. The silver particle agglomeration has dispersants, surfactants, and polymers

#228743 - $15.00 USD Received 28 Nov 2014; revised 30 Jan 2015; accepted 18 Feb 2015; published 25 Feb 2015

for smooth jetting. The printed silver nanoparticle ink has low conductivity because of impurities. In order to attain high conductivity after printing, a sintering process is necessary for burning off impurities. Furthermore, sintering processes increase bonding to the substrate. There are several sintering processes, such as thermal, ultraviolet (UV) flashlight, and laser processes. In this study, the thermal sintering process has been used because of its efficiency and simplicity. Higher conductivity can be attained by increasing the sintering temperature for a suitable time [14]. To fabricate a sample absorber, a commercial inkjet printer (EPSON WF-7011), a low-cost flexible polyethylene-terephthalate (PET) based polymer film (Novacentrix Novele IJ-220), and a silver nanoparticle ink (Novacentrix JS-B25P) are used. The resolution of the printer is 5760 × 1440 dpi. When the designed width and gap are 0.1 mm, the printed width and gap are 192 um and 112 um as shown in Fig. 3(a) and (b), respectively. It is observed that the maximum printing error is 12 um. We use three sheets of the polymer film for the flexible substrate and attach these sheets using non-conductive epoxy. To determine the substrate's electrical characteristics, the T-resonator method [15] is used. The substrate's measured relative permittivity and dielectric loss tangent are 2.66 and 0.024, respectively. The required printing time for the sample absorber is less than 90 seconds, which, compared with the printed circuit board (PCB) manufacturing process, is relatively faster. The thin-film sheet resistance of the silver nanoparticle ink is 60 mΩ. The conductivity of the silver nanoparticle ink is about 31% of the conductivity of bulk silver (6.3×10^7 S/m) and is higher than the conductivity of bulk iron (1.0×10^7 S/m). Scanning electron microscope (SEM) images of the printed pattern (before and after sintering) are shown in Fig. 2. Because metallic ink particles are very small, their melting points are much lower than the melting points of bulk metals [14]. After being subjected to a 120°C thermal sintering process for an hour, nanoparticles combine with each other and become a conductive layer.

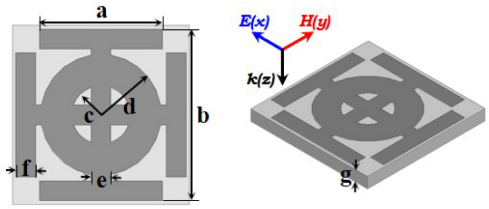

Fig. 1. Unit cell of the proposed absorber with a = 4.7 mm, b = 6.5 mm, c = 1.11 mm, d = 2.3 mm, e = 0.75 mm, f = 0.75 mm, and g = 0.62 mm.

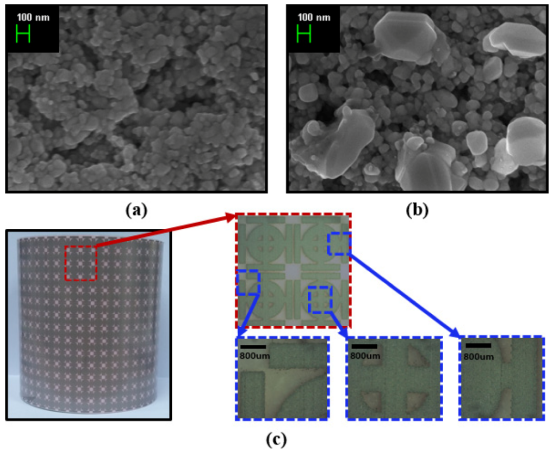

Fig. 2. SEM images (a) before sintering and (b) after sintering; (c) the fabricated sample absorber coated on a PET cylinder and a microphotograph of the sample absorber.

#228743 - $15.00 USD Received 28 Nov 2014; revised 30 Jan 2015; accepted 18 Feb 2015; published 25 Feb 2015

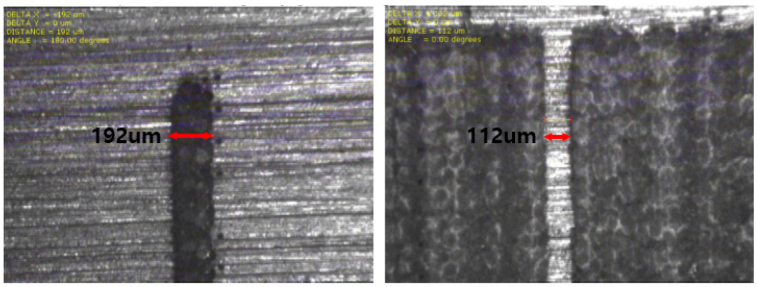

Fig. 3. Microscopic images of the inkjet-printed (a) line and (b) gap on the film substrate.

The proposed unit cell is motivated by the angular-insensitive ring resonator in Fig. 4(a) [16]. In order to reduce its electrical size, the unit cell of Fig. 4(a) is modified by introducing four outermost arms. As shown in Fig. 4(c), the reflection coefficient of the proposed unit cell (Fig. 4(b)) is compared with that of the primitive unit cell (Fig. 4(a). Although their size (b) is same, the resonant frequency of the proposed unit cell is lower than that of the primitive unit cell. When length (a) is increased, inductance is increased so that the resonant frequency becomes lower as shown in Fig. 4(d). Instead of gap capacitance of the primitive design, we can generate higher capacitance from capacitance between adjacent outermost arms.

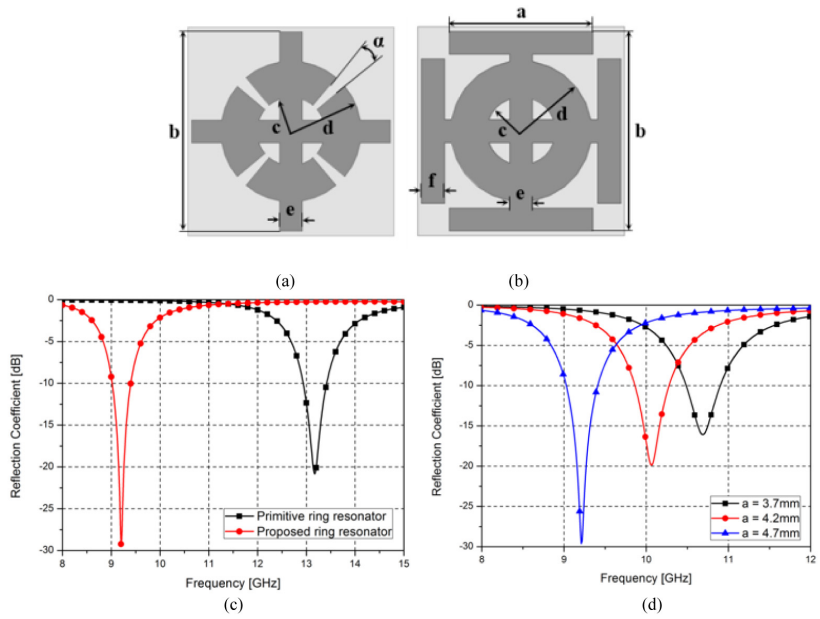

Fig. 4. (a) Primitive ring resonator, (b) proposed ring resonator (a = 4.7 mm, b = 6.5 mm, c = 1.11 mm, d = 2.3 mm, e = 0.75 mm, f = 0.75 mm, g = 0.62 mm, and α = 10þ), (c) simulated reflection coefficients of (a) and (b), and (d) reflection coefficients of the proposed unit cell when a is 3.7 mm, 4.2 mm, and 4.7 mm.

High absorption in metamaterial can be achieved by eliminating both transmitted and reflected wave. The reflected wave can be eliminated by matching the impedance of the metamaterial absorber to the impedance of free space. To eliminate the transmitted wave, the transmitted wave's energy needs to be dissipated through conductive and dielectric losses. To achieve zero reflection, it is necessary to manipulate the permittivity (ε) and permeability (μ)

#228743 - $15.00 USD Received 28 Nov 2014; revised 30 Jan 2015; accepted 18 Feb 2015; published 25 Feb 2015

of the metamaterial because the intrinsic impedance (η) depends on the permittivity and permeability of the medium ($\eta = \sqrt{\mu / \varepsilon}$). By manipulating the permittivity and permeability, we produce perfect impedance matching with the free space around the metamaterial. In addition, the refractive index (*n*) of the metamaterial has a large imaginary part, which describes the loss component and allows for high absorptivity. Therefore, if the metamaterial is perfectly matched to the surrounding free space with sufficient loss, it shows high absorptivity even though a low profile. In order to retrieve the effective parameters for a complex metasurface, phase of transmission and reflection coefficients are required. Recently, indirect and direct characterization techniques of complex optical metasurfaces have been developed in order to obtain phases of transmission and reflection coefficients [17], [18]. In this work, phase of transmission and reflection coefficients is directly measured using a waveguide method by a vector network analyzer because the proposed metamaterial is working in microwave region [19]. In Fig. 5, the complex impedance of the proposed metamaterial is plotted versus frequency after normalizing to the impedance of free space. It is observed that the normalized impedance is close to one at 9.21 GHz which represents impedance matching to free space. The relative permittivity and relative permeability are related to both the refractive index and the normalized intrinsic impedance by the relations

$$\varepsilon_r = n / \eta, \ \mu_r = n\eta \tag{1}$$

The refractive index and intrinsic impedance be can calculated using S parameters [20], as given by

$$n = \frac{1}{kg}\cos^{-1}\left[\frac{1}{2S_{21}}(1 - S_{11}^{\ 2} + S_{21}^{\ 2})\right] \tag{2}$$

$$\eta = \sqrt{\frac{(1+S_{11})^2 - S_{21}^{\ 2}}{(1-S_{11})^2 - S_{21}^{\ 2}}}, \tag{3}$$

where *k* is the wave number and *g* can be found in Fig. 1.

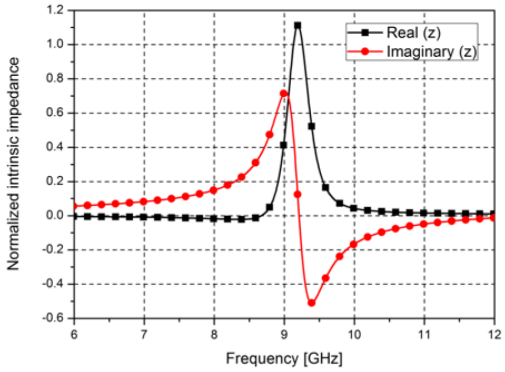

Fig. 5. Normalized impedance of the proposed metamaterial absorber versus frequency.

A metamaterial perfect absorber is realized with simultaneous electric and magnetic resonances [4]. In addition, transmission is minimized by high loss of the metamaterial. In order to generate electric and magnetic resonances, a bi-layered metal structure is necessarily. Figures 6(a) and (b) demonstrates electric resonance and magnetic resonance, respectively. Top and bottom layers of metal structure provide electrical response. It is observed in Fig. 6(a) that electric fields are concentrated strongly in the edges. Magnetic resonance is observed from surface current densities in Fig. 6(b) where the surface currents excited in the

#228743 - $15.00 USD Received 28 Nov 2014; revised 30 Jan 2015; accepted 18 Feb 2015; published 25 Feb 2015

two metal layers are anti-parallel. In addition, high loss of the metamaterial is verified by volume loss densities in Fig. 6(c). Total losses can be increased by making the dielectric material thicker. Consequently, the electric and magnetic resonance can be individually adjusted by changing the resonator pattern and the thickness of the dielectric material, respectively. Transmission can be also minimized by increasing thickness of the dielectric material.

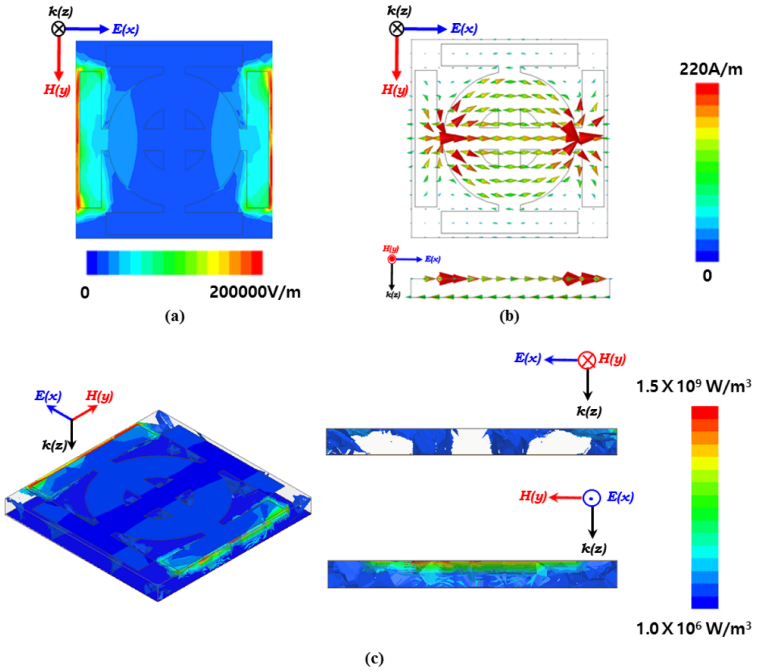

Fig. 6. (a) Simulated electric field distribution, (b) vector current density, and (c) volume loss density in the proposed absorber.

3. Simulated and measured results

To verify the absorption of the proposed absorber, 40 × 14 unit cells are printed on a 27.2-cm × 9.5-cm film substrate and coated on a PET cylinder with a 4.56-cm radius. Figure 8 depicts the experimental setup for our measurements. An Anritsu MS2038C vector network analyzer and two standard gain horn antennas are used to transmit EM waves and to receive reflected signals from the sample absorber. Wedge-tapered absorbers are used to prevent unwanted reflection, and a time-gating method is used with the vector network analyzer to measure only the reflected signal from the sample absorber. The distance between the sample absorber and the antennas is 1 m, which satisfies the far-field condition. Before measuring the sample absorber's reflection coefficient, we measure the reflection coefficient of the copper plate (which has dimensions identical to the sample absorber) for measurement reference $\Gamma = -1$. For the cylindrical absorber's measurement reference, we cover the same cylinder with a copper sheet.

#228743 - $15.00 USD Received 28 Nov 2014; revised 30 Jan 2015; accepted 18 Feb 2015; published 25 Feb 2015

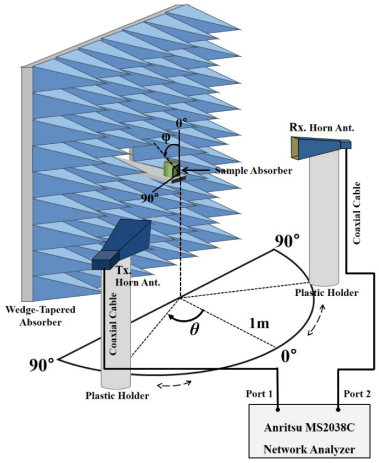

Fig. 7. Experimental setup for measurements.

The absorptivity $A(\omega)$ can be calculated using the reflection coefficient $R(\omega)$ and transmission coefficient $T(\omega)$, and is given by

$$A(\omega) = 1 - R(\omega) - T(\omega) \tag{4}$$

The bottom layer of the sample absorber is fully covered with the conductive sheet, which ensures that there are no transmission waves. Consequently, we can ignore the transmission and calculate the absorption by measuring the reflection coefficient.

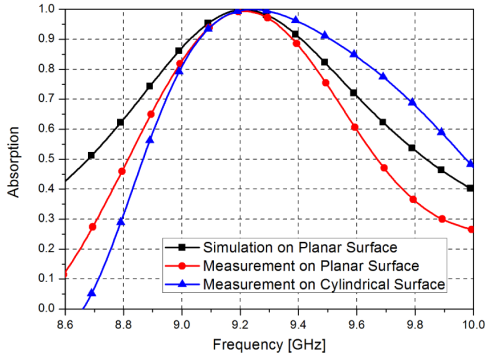

Fig. 8. Numerical simulation and measured results for a vertical polarized wave.

The HFSS simulation, the measured absorption result for the planar absorber model, and the measured result for the cylindrical absorber model for the vertically polarized incident wave are shown in Fig. 8. At 9.21 GHz, the simulation and the measurement results for both absorber models show an absorption rate exceeding 99%, and the results are in good agreement at the resonant frequency. Slight difference is due to finite size of the array because the simulated result is obtained from infinite periodic structure. However, the fabricated array size is large enough to achieve similar absorptivity with the simulated result in the present measurement setup (Fig. 7).

In Table 1, we compared the performances of the proposed inkjet-printed metamaterial absorber with other metamaterial absorbers fabricated in optical lithography and printed circuit board (PCB) technology. It is observed that the proposed absorber shows similar or even better absorptivity and bandwidth.

#228743 - $15.00 USD Received 28 Nov 2014; revised 30 Jan 2015; accepted 18 Feb 2015; published 25 Feb 2015

Table 1. Comparison of the proposed inkjet-printed metamaterial performances with other technology

Research paper	Fabricate Technique	Resonant frequency	Absorptivity	Bandwidth (over 80% absorption)
Reference [4]	Optical lithography	11.48GHz	88%	0.3GHz (2.6%)
Reference [16]	Optical lithography	10.91GHz	99%	0.4GHz (3.7%)
Reference [21]	PCB	9.5GHz	90%	0.25GHz (2.6%)
Reference [22]	PCB	10.14GHz	95%	0.25GHz (2.5%)
Proposed work	Inkjet-printing	9.21GHz	99%	0.4GHz (4.3%)

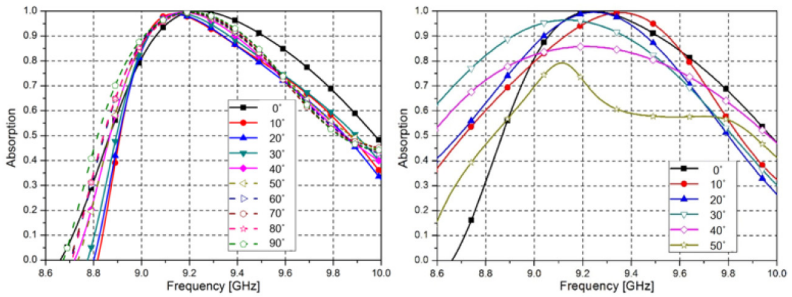

Fig. 9. (a) Measured absorption rates for different polarization angles (φ is varied from 0þ to 90þ) and (b) different incident angles (θ is varied from 0þ to 90þ).

Measured polarization and incident angle dependence of the cylindrical absorber is also investigated. To measure absorption ratios at different polarization, one horn antenna is placed in front of the sample absorber (normal incidence of θ = 0þ) to measure different polarization angles φ of the sample absorber. We rotate a polarization angle (φ) from 0þ to 90þ and measure the reflection coefficient in 10þ increments. In Fig. 9(a), the measured results for the polarization sensitivity are plotted. At 9.21 GHz, the absorption rates for all polarization angles exceed 96% because of the symmetric top layer pattern. To measure absorption ratios at different incident angles absorber (θ), two standard gain horn antennas are used to change incident wave angles. Based on Snell's law, two horn antennas are placed at the same angle (θ). The measurement results are plotted in Fig. 9(b). The results indicate an absorption rate exceeding 95% at 9.21 GHz when angle θ is lower than 30þ, and when incident angle θ becomes 40þ, the absorption rate becomes 85.8%.

4. Conclusion

We have successfully printed the sample absorber on the flexible polymer film with a commercial printer. Compared with the PCB process, this procedure is simple, fast, economical, and environmentally friendly. The printed sample absorber is deployed on a PET cylinder of radius 4.56 cm. At 9.21 GHz, both the planar and cylindrical models achieve an absorption rate exceeding 99%. In addition, the cylindrical model attains an absorption rate higher than 96% for all polarization angles and achieves an absorption rate over 95% when the incident angle is lower than 30þ.

Acknowledgments

This work was supported by the National Research Foundation of Korea (NRF) grant funded by the Korea government (MSIP) (No.2014R1A2A1A11050010).

#228743 - $15.00 USD Received 28 Nov 2014; revised 30 Jan 2015; accepted 18 Feb 2015; published 25 Feb 2015